

Corrosion Inhibition Effect of Phosphate on Fine-grain High-strength Reinforcement in Simulated Concrete Pore Solutions with Carbonation and Chloride-intrusion

Bilan Lin^{1,2,*}, Chaonong Liu¹, Zan Luo¹, Jieda Li¹, Shan Wang¹, Yuye Xu³

¹ School of Material Science and Engineering, Xiamen University of Technology, Xiamen 361024, China

² Key Laboratory of Functional Materials and Applications of Fujian Province, Xiamen 361024, China

³ College of Civil Engineering, Huaqiao University, Xiamen, Fujian 361021, China

*E-mail: linbilan@xmut.edu.cn

Received: 16 December 2016 / Accepted: 12 January 2017 / Published: 12 February 2017

The passivation performance of fine-grain high-strength (HRBF500) reinforcement in simulated concrete pore (SCP) solutions was seriously impaired by carbonation and chloride-intrusion of concrete. Phosphate was used as corrosion inhibitor and the effect of $[\text{PO}_4^{3-}]/[\text{Cl}^-]$ ratio was investigated. The corrosion properties of HRBF500 reinforcement were investigated via potentiodynamic polarization, electrochemical impedance spectroscopy (EIS) and scanning electron microscopy (SEM). The semiconductor features of the corrosion products were studied according to Mott–Schottky theory. The results show that the anodic corrosion process of HRBF500 reinforcement can be greatly inhibited by sufficient high phosphate concentration, while the influence on the cathodic process is generally smaller. The corrosion products on HRBF500 reinforcement manifest as n-type semiconductors. With the increase in $[\text{PO}_4^{3-}]/[\text{Cl}^-]$ ratio, the donor concentration N_D decreases, while the efficiency of corrosion protection first increases considerably and then tends to be stable. The compactness of the corrosion products is also enhanced. For the case with $0.6 \text{ mol}\cdot\text{L}^{-1} \text{ Cl}^-$ but without carbonation ($\text{pH} \approx 12.5$), the corrosion current density i_{cor} decreases from 13.2 to $0.40 \mu\text{A}\cdot\text{cm}^{-2}$ at $[\text{PO}_4^{3-}]/[\text{Cl}^-] = 1.0$, while for $\text{pH} = 10.5$ and $[\text{Cl}^-] = 0.3 \text{ mol}\cdot\text{L}^{-1}$ (more aggressive), i_{cor} is still up to $0.80 \mu\text{A}\cdot\text{cm}^{-2}$ and decreases to $0.42 \mu\text{A}\cdot\text{cm}^{-2}$ at $[\text{PO}_4^{3-}]/[\text{Cl}^-] = 4.0$. Therefore, to obtain better corrosion protection under the combined action of carbonation and chloride-intrusion, a higher phosphate concentration is required.

Keywords: Reinforcement; Fine grain; Corrosion; Simulated concrete pore solution; Phosphate

1. INTRODUCTION

Fine-grain high-strength steel, due to its finer grain, more uniform microscopic structure, fewer alloys and fewer impurities, is a good representation of the use of an advanced high-performance

material in the 21st century [1-3]. The main strengthening techniques are micro-alloying with Nb, V and Ti and thermo-mechanical control processing, which enhance both strength and ductile plasticity to a high degree. Application of fine-grain high-strength steel in various engineering is favorable to economic savings, reduction in resource consumption and alleviation of environmental burdens. It is also beneficial for the sustainable development of materials and to promote the ‘greening’ of building construction. Thus, it has been widely used in coastal construction projects, bridges, heavy steel structures, high-speed railways, oil and gas pipelines, boilers, pressure vessels, ships, etc [3-5]. Fine-grain high-strength steel with yield strength of 500 MPa is the dominant reinforcement material used in civil engineering structures in China. It is referred to as HRBF500 [6], where “HRB” refers to the “Hot-rolled Ribbed Bar”, “F” refers to the “Fine-grain”, and “500” refers to the yield strength (the unit is “MPa”). Recently, the mechanical properties of HRBF500 reinforcement and the seismic and fire resistance of the casted concrete members have been systematically investigated [7-9]. However, its corrosion behavior has rarely been examined [10].

Under normal conditions, the concrete is highly alkaline ($\text{pH} = 12\sim 13$), thus the reinforcement is passivated according to the $E\text{-pH}$ equilibrium diagram of the $\text{Fe-H}_2\text{O}$ system [11, 12]. However, the protective passivation film on the surface of the reinforcement is damaged following carbonation and chloride-intrusion of the concrete and is thereby corroded. Moreover, the corrosion of the metal is closely related to grain size, morphology, impurities, etc [13, 14].

Recently, corrosion and protection of plain-round carbon steel (commonly referred to as HPB235) and HRB335 (“Hot-rolled Ribbed Bar” with a yield strength of “335” MPa) reinforcement, which are, respectively, the first and second generations of reinforcement, have been comprehensively studied [15-19]. However, few papers have reported the corrosion of high-strength or fine-grain reinforcement [20-22]. Mohammed et al. [21] found that ribbed reinforcement is more sensitive to corrosion than plain-round reinforcement. Jiang et al. [22] compared the corrosion of HRB335, HRB400 and HPB235 reinforcements in chloride-intruded concrete and found that the corrosion rates of the first two are considerably greater than that of HPB235. There are macro-corrosion cells on the lined sets between different reinforcements [23]. Li et al. [24] also found that the corrosion behavior of HRB335 and HPB235 reinforcements in concrete with fly ash is almost similar, but the corrosion rate of the former is greater. Thus, it is conjectured that the corrosion resistance of HRB reinforcement, with a relatively greater strength, might be inferior to that of HPB reinforcement.

As far as fine-grain reinforcement is concerned, a greater number of (fine) grain boundaries may also lead to a decrease in corrosion resistance in aggressive environments [10, 20, 25, 26]. Shi et al. [20, 25] found that the stability of the passivation film on fine-grain reinforcement in SCP solution without chloride ions is better than that of HPB235 reinforcement. However, the pitting corrosion of the former is conversely more serious than that of the latter in the presence of chloride. The authors found that the corrosion sensitivity of HRB500 and HRB400 reinforcements to carbonation and chloride in SCP solution is greater than that of HPB235 [27, 28] and the corrosion inhibition effect of nitrite on HRBF500 is poorer than that on HPB235 [10]. Even inhibitors such as benzotriazole and phytic acid, which are very effective for HPB235 reinforcement, are completely useless for HRBF500 reinforcement [26, 29, 30]. Therefore, the need for studies on the corrosion behavior of HRBF500 reinforcement, different from traditional reinforcements, is pressing.

Inhibitors are one of the most common and effective approaches to alleviate the corrosion of reinforcements [31-33]. Phosphate is an environmental friendly and economic inhibitor for metals [34-36] and acts via the well-known mechanism of anodic inhibition [37, 38]. However, some studies found that phosphate sometimes conducts as a cathodic or mixed inhibitor, correlated with the $[\text{PO}_4^{3-}]/[\text{Cl}^-]$ ratio [34, 39]. In recent years, phosphate has also been used to inhibit the corrosion of reinforcements in SCP solution or concrete media [16, 34, 40-42]. However, the effects of phosphate on fine-grain or high-strength reinforcements in alkaline concrete media have not yet been reported. In this study, sodium phosphate was used as the corrosion inhibitor for HRBF500 reinforcement in SCP solutions with different chloride concentrations and different amounts of carbonation. The influence of various $[\text{PO}_4^{3-}]/[\text{Cl}^-]$ ratios was also investigated, as well as the electrochemical corrosion behavior, the semiconductor characteristics and the microscopic structure of the corrosion products. Finally, the inhibition mechanism is discussed.

2. EXPERIMENTAL

2.1 Materials and electrodes

The materials tested were cut using a linear cutting machine from HRBF500 reinforcement with a diameter of 16 mm. The metallographic structure was compared to that of HPB235 reinforcement [10], as shown in Fig. 1. The microscopic structure of HRBF500 reinforcement, including bright ferrite and gray pearlite, is finer and more uniform. The bright ferrite content is largely greater than that of HPB235 reinforcement, indicating that the carbon content of the former is lower. Conversely, the gray pearlite content of HPB235 reinforcement is extremely large and heterogeneous. Thus, the strength and ductility of HRBF500 reinforcement is greatly superior to that of HPB235.

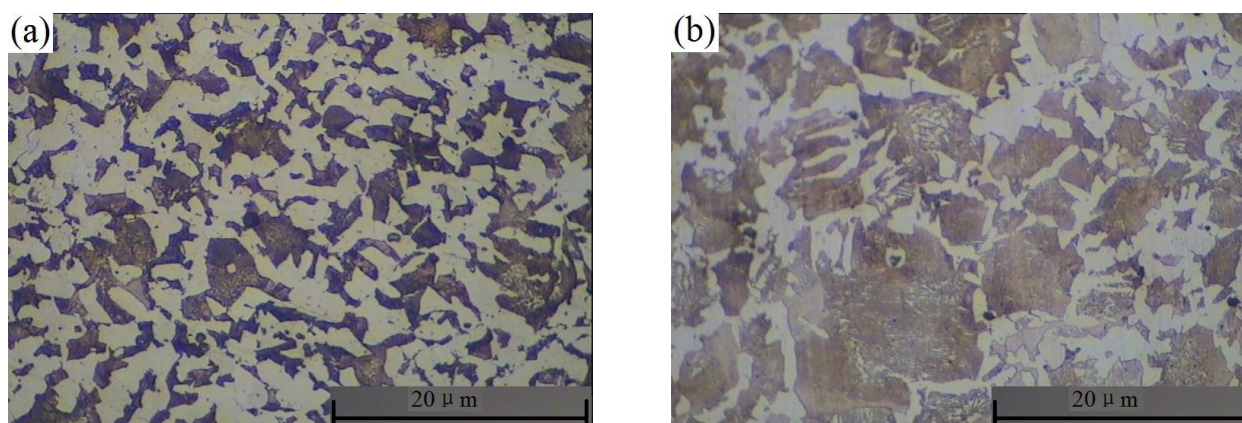


Figure 1. Metallographs of (a) HRBF500 and (b) HPB235 reinforcements

One end of the HRBF500 reinforcement served as the working surface of the electrode, with an exposed area of 2.01 cm^2 , while a copper wire was welded to the other end. Except for the working

surface, all parts of the working electrode were sealed with epoxy resin. The naked surface was first polished sequentially with waterproof abrasive papers (Nos. 200–2000), subsequently cleaned ultrasonically with absolute ethanol, then rinsed with de-ionized water and finally dried in a stream of cool air.

2.2 Tested solutions

A supersaturated calcium hydroxide solution, allowed to stand for 24 h, served as the SCP solution and had a pH of about 12.5. Sodium bicarbonate and sodium chloride were added to simulate carbonation (i.e. decreasing pH) and chloride-intrusion of the SCP solution, respectively. Based on the previous studies [27, 28], four typical cases for HRBF500 reinforcement were tested, as shown in Table 1. Case *I* is the pure and uncontaminated case; Case *II* is chloride-intrusion with $0.6 \text{ mol}\cdot\text{L}^{-1}$ of chloride ions; Case *III* is carbonation of concrete with a pH of 10.5; Case *IV* simulates the combined action of carbonation and chloride-intrusion.

Table 1. Four corrosion cases to simulate carbonation and chloride-intrusion of the SCP solution

Case ID	pH	$[\text{Cl}^-]/\text{mol}\cdot\text{L}^{-1}$	Instructions
<i>I</i>	12.5	0.0	Pure, without any contaminant
<i>II</i>	12.5	0.6	Cl^- -intrusion only, without carbonation
<i>III</i>	10.5	0.0	Carbonation only, without Cl^- -intrusion
<i>IV</i>	10.5	0.3	Combined action of carbonation and Cl^- -intrusion

Phosphate ions (PO_4^{3-}) were introduced by means of sodium phosphate ($\text{Na}_3\text{PO}_4\cdot 12\text{H}_2\text{O}$). To examine the corrosion inhibition of phosphate for HRBF500 reinforcement under conditions of carbonation and/or chloride-intrusion the $[\text{PO}_4^{3-}]/[\text{Cl}^-]$ ratio was varied, where $[\text{PO}_4^{3-}]$ and $[\text{Cl}^-]$ represent the molar concentrations of phosphate ions and chloride ions, respectively. $[\text{PO}_4^{3-}]/[\text{Cl}^-]$ ratios of 0, 0.1, 0.2, 0.4, 0.6, 0.8 and 1.0 were used in Case *III* and ratios of 0, 0.1, 0.6, 1.0, 2.0 and 4.0 were used in Case *IV*.

2.3 Electrochemical measurements

All electrochemical tests were conducted using a CHI604E electrochemical workstation employing a conventional three-electrode system. A saturated calomel electrode (SCE) was used as the reference electrode, to which all potentials reported in this paper are referred, while a platinum electrode served as the counter-electrode. The working electrode was the HRBF500 reinforcement.

After a steady open-circuit potential was obtained for approximately one hour immersion in the SCP solution, the electrochemical measurements, including potentiodynamic polarization, electrochemical impedance spectroscopy (EIS) and impedance–potential plots, were made.

EIS measurements were performed at a stable open-circuit potential. The amplitude of the AC potential signal was 5 mV. The frequency ranged from 100 kHz to 10 mHz.

The potentiodynamic polarization tests were run from -0.6 V and were stopped when the anodic current density reached $100 \mu\text{A}\cdot\text{cm}^{-2}$ [16]. The scan rate was $1 \text{ mV}\cdot\text{s}^{-1}$. The corrosion potential E_{cor} , the corrosion current density i_{cor} , the breakdown potential E_b and the cathodic Tafel slope b_c were obtained from the tested polarization curves. To determine the inhibition efficiency of phosphate for HRBF500 reinforcement in corrosive media, the corrosion protection efficiency P_e was calculated from the expression

$$P_e(\%) = \left(1 - \frac{i_{\text{cor}}}{i_{\text{cor}}^0}\right) \times 100 \quad (1)$$

where i_{cor}^0 and i_{cor} are the corrosion current densities of HRBF500 reinforcement in SCP solution without and with phosphate inhibitor, respectively. The $[\text{PO}_4^{3-}]$ values in Case III were 0.06, 0.12, 0.24, 0.36 and $0.48 \text{ mol}\cdot\text{L}^{-1}$ and those in Case IV were 0.03, 0.18, 0.30, 0.60 and $1.20 \text{ mol}\cdot\text{L}^{-1}$.

Generally, the passivation film or the corrosion products on reinforcement in concrete are made up of various iron oxides [10, 43, 44], so they have the features of a semiconductor [45]. In this study, the impedance–potential curves were first measured with the test potential varying from -0.6 V to 0.6 V; the potential increment was 10 mV. The frequency and amplitude of the AC potential signal were 1000 Hz and 10 mV, respectively. Based on Mott–Schottky theory [42, 43], the relationship between $1/C_{\text{sc}}^2$ and E for different types of semiconductor can be expressed as:

$$\text{n-type: } \frac{1}{C_{\text{sc}}^2} = \frac{2}{\epsilon_0 \epsilon \epsilon N_{\text{D}}} \left[E - E_{\text{fb}} - \frac{kT}{e} \right] \quad (2)$$

$$\text{p-type: } \frac{1}{C_{\text{sc}}^2} = -\frac{2}{\epsilon_0 \epsilon \epsilon N_{\text{A}}} \left[E - E_{\text{fb}} - \frac{kT}{e} \right] \quad (3)$$

where C_{sc} is the capacitance of the space charge layer, ϵ_0 is the vacuum dielectric constant ($8.854 \times 10^{-12} \text{ F}\cdot\text{m}^{-1}$), ϵ is the relative dielectric constant (about 12 for iron oxides [45]), e is the electron charge ($1.602 \times 10^{-19} \text{ C}$), N_{A} and N_{D} are the acceptor and donor concentrations for p-type and n-type semiconductors, respectively, E is the electrode potential, E_{fb} is the flat band potential, k is the Boltzmann constant ($1.38066 \times 10^{-23} \text{ J}\cdot\text{K}^{-1}$), T is the thermodynamic temperature, and kT/e is about 25 mV at room temperature and can be taken as negligible in the formulas above. When the slope of the Mott–Schottky curve (i.e. $1/C_{\text{sc}}^2 \sim E$ plots) is positive, the film is an n-type semiconductor.

Conversely, when the slope is negative, it is p-type. Based on the slope and intercept calculated from linear fitting, N_{A} , N_{D} and E_{fb} can be obtained.

2.4 Surface analysis

The surface morphology of HRBF500 reinforcement after immersion in various SCP solutions for six hours was analyzed by scanning electron microscopy (SEM) (EVO-18, Zeiss) and energy-dispersive X-ray spectroscopy (EDS) (X-MAX 20, Oxford Instruments).

3. RESULTS AND DISCUSSION

3.1 Corrosion of HRBF500 reinforcement in the four cases

Figure 2 presents the effects of chloride-intrusion and carbonation on potentiodynamic polarization curves for HRBF500 reinforcement in four SCP solutions. The corresponding morphology of the passivation film and/or corrosion products on the surface of HRBF500 reinforcement is shown in Fig. 3.

In Case I (i.e. pure SCP solution, Fig. 2), the cathodic corrosion process of HRBF500 reinforcement displays an activation polarization control, namely, the consumption of electrons by oxygen is the slowest step, while typical passivation characteristics are manifested on the anodic polarization branch – the passivation region is broad and stable. The breakdown potential of the passivation film E_b is approximately 0.62 V and the passivation retaining current density i_{pass} is about $27.5 \mu A \cdot cm^{-2}$. This can be attributed to a compact passivation film formed on the surface of HRBF500 reinforcement, as shown in Fig. 3(a). Based on EDS analysis, the oxygen content is higher, indicating that the passivation film is likely composed of oxides and hydroxides of iron [43, 44].

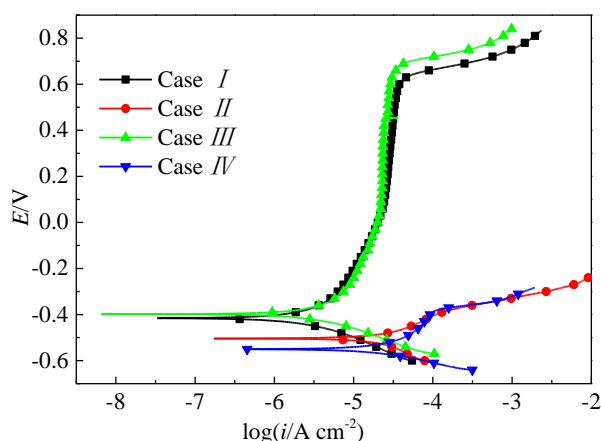
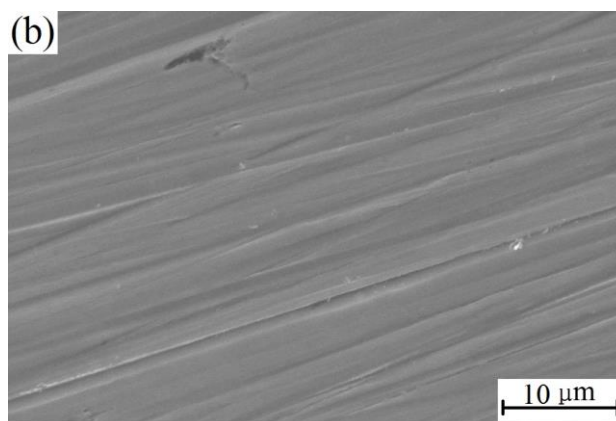
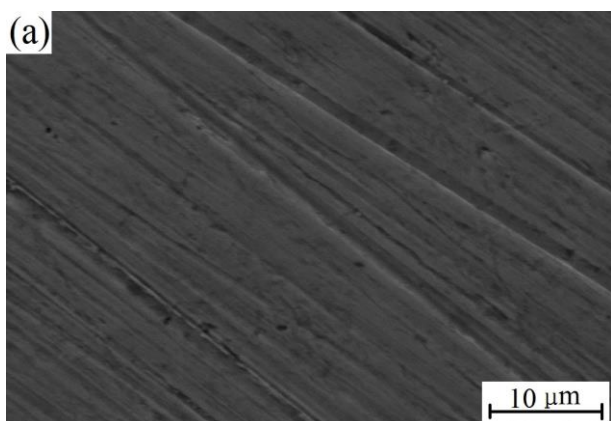


Figure 2. Potentiodynamic polarization curves for HRBF500 reinforcement in four cases



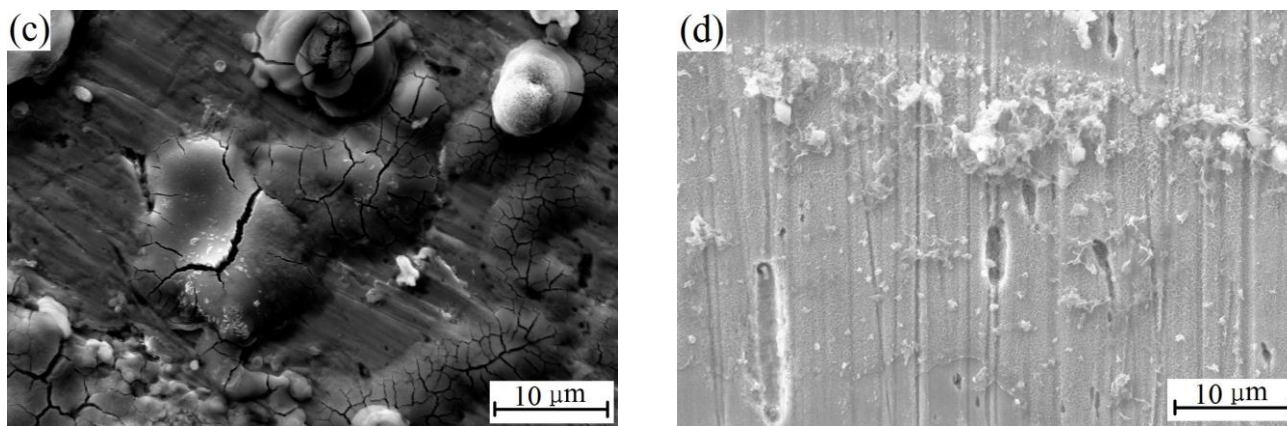


Figure 3. SEM images of HRBF500 reinforcement immersed in four different SCP solutions: (a) Case I, (b) Case II, (c) Case III, (d) Case IV

As shown in Fig. 2, when the SCP solution was carbonized to pH = 10.5 and chloride ions were not intruded (Case II), the corrosion performance of HRBF500 reinforcement was very similar to that in the pure SCP solution. The cathodic process, i.e. reduction of oxygen, is also the activation polarization control, and the anodic process is a steady passivation of the reinforcement. The surface of HRBF500 reinforcement is smooth, and a complete and compact film containing a greater quantity of oxygen is formed (Fig. 3(b)).

However, there are also some differences between Case II and Case I (Fig. 2). The cathodic polarization branch in Case II is shifted slightly towards the right. The carbonation of the SCP solution slightly accelerates the consumption of electrons by oxygen on the surface of HRBF500 reinforcement, while the E_b value reaches 0.69 V, considerably higher than that in Case I. The breakdown of the passivation film is also called the transpassivation of metals, and a new oxidation reaction takes place. That is, hydroxide ions are oxidized to oxygen atoms, which can be expressed as [37]:



With a decrease in pH value, the molar concentration of hydroxide ions, i.e. $[OH^-]$, also decreases. The temperature (T) and the pressure of oxygen (P_{O_2}) remained almost invariant during the electrochemical measurements. According to the Nernst equation, the equilibrium potential of the above forward reaction, $E_e(OH^- / O_2)$ can be calculated as

$$E_e(OH^- / O_2) = E_e^\theta(OH^- / O_2) + \frac{RT}{4F} \ln \frac{[OH^-]^4}{P_{O_2}} \tag{5}$$

where R and T have the same meaning as in Mott–Schottky theory, F is the Faraday constant (about 96500 C) and $E_e^\theta(OH^- / O_2)$ is the equilibrium potential of the forward reaction under standard state conditions. Therefore, $E_e(OH^- / O_2)$ increases with a decrease in pH value, leading to an increase in E_b . Therefore, the oxidation reaction of hydroxide ions to oxygen atoms becomes more difficult when concrete is carbonized.

As shown in Figs. 2 and 3, when a certain concentration of chloride ions was added to SCP solutions without and with carbonation (Cases *III* and *IV*, respectively), the corrosion behavior of HRBF500 reinforcement changes radically. The cathodic corrosion process is still controlled by the activation polarization, but the anodic passivation disappears and the anodic polarization branch shifts towards the right. HRBF500 reinforcement in this case is at a state of activation dissolution. Moreover, the corrosion current density i_{cor} in Case *IV* is about $37.9 \mu\text{A}\cdot\text{cm}^{-2}$, markedly higher than that in Case *III* (about $13.2 \mu\text{A}\cdot\text{cm}^{-2}$). The chloride ion concentration in Case *IV* is half that in Case *III*, but the corrosion of HRBF500 reinforcement is seriously aggravated.

In Case *III*, there are numerous corrosion products on the surface of HRBF500 reinforcement (Fig. 3(c)). The worm spots and convex points are cracked and contain a high content of chloride based on EDS analysis. The flat surfaces contain more oxygen but contain no chloride. However, in Case *IV* the surface morphology of HRBF500 reinforcement is obviously different (Fig. 3(d)), there are some flocculent and loose corrosion products, pitting corrosion is extremely serious, and the pit size is highly variable. The smaller pits are less than $1 \mu\text{m}$, while some large pits are greater than $15 \mu\text{m}$. According to EDS analysis, the flocculent corrosion products contain a large amount of chloride, while the pits and the flat surface contain almost no chloride. This further illustrates the severe corrosion of HRBF500 reinforcement under the combined action of carbonation and chloride-induction of concrete. In the next section, the effect of $[\text{PO}_4^{3-}]/[\text{Cl}^-]$ ratio on the corrosion performance of HRBF500 reinforcement in these two aggressive conditions, i.e. Cases *III* and *IV*, will be discussed further.

3.2 Effect of $[\text{PO}_4^{3-}]/[\text{Cl}^-]$ ratio - potentiodynamic polarization curves

The effect of $[\text{PO}_4^{3-}]/[\text{Cl}^-]$ ratio on potentiodynamic polarization curves of HRBF500 reinforcement in Cases *III* and *IV* is shown in Fig. 4. With phosphate present in both cases, the cathodic corrosion process is also controlled by the activation polarization and the cathodic branch moves towards the left. This shift degree increases with $[\text{PO}_4^{3-}]/[\text{Cl}^-]$ ratio. In Case *III* the shift is slightly larger. The reduction reaction of oxygen on the surface of HRBF500 reinforcement can be inhibited by phosphate, and the suppression is marginally larger in Case *III*.

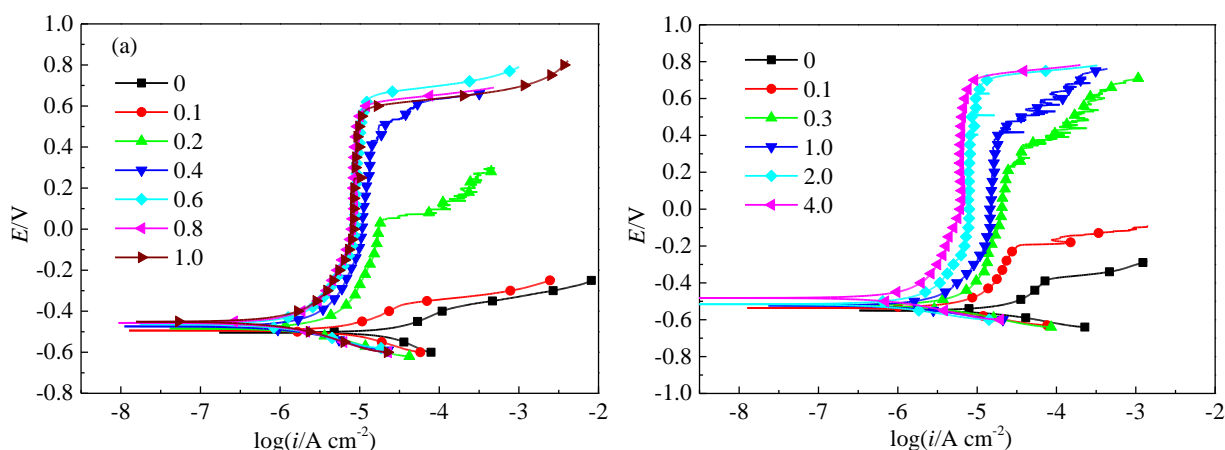


Figure 4. Effect of $[\text{PO}_4^{3-}]/[\text{Cl}^-]$ ratio on polarization curves for HRBF500 reinforcement in: (a) Case *III*, (b) Case *IV*

The anodic polarization branch is also shifted to the left in the presence of phosphate (Fig. 4). The amplitude of this shift is greater than that of the cathodic branch under the same conditions, which indicates that phosphate acts mainly as an anodic corrosion inhibitor [36-38]. There are also differences in the changes of the anodic branch with changes in $[\text{PO}_4^{3-}]/[\text{Cl}^-]$ ratio in Cases *III* and *IV*. In Case *III*, the extent of the shift to the left is not obvious at first but is then considerable for $[\text{PO}_4^{3-}]/[\text{Cl}^-]$ ratios ranging from 0 to 0.2. With further increase in $[\text{PO}_4^{3-}]/[\text{Cl}^-]$ ratio to 0.4, the degree of shift to the left slows down but the passivation region continues to widen. For $[\text{PO}_4^{3-}]/[\text{Cl}^-]$ ratios up to 0.6, the anodic branch remains almost unchanged and a wide and stable passivation region is clearly seen. In Case *IV*, however, the anodic branch is gradually shifted to the left with an increase in $[\text{PO}_4^{3-}]/[\text{Cl}^-]$ ratio from 0 to 2.0, and finally a broad and stable passivation region is established for a $[\text{PO}_4^{3-}]/[\text{Cl}^-]$ ratio of 4.0.

The corrosion of HRBF500 reinforcement in SCP solutions with chloride and carbonation is greatly inhibited by phosphate and, with sufficiently high phosphate concentration, a more stable and compact passivation film on HRBF500 reinforcement is formed. For example, the tested minimum values of i_{pass} for HRBF500 reinforcement in Cases *III* and *IV* were, respectively, 8.42 and 6.21 $\mu\text{A}\cdot\text{cm}^{-2}$, remarkably smaller than the 27.5 $\mu\text{A}\cdot\text{cm}^{-2}$ in the uncontaminated SCP solution. The corresponding maximum values of E_b were up to 0.64 and 0.69 V, higher than the 0.62 V in Case *I*.

Table 2. Effect of $[\text{PO}_4^{3-}]/[\text{Cl}^-]$ ratio on polarization parameters for HRBF500 reinforcement in Case *III*

$[\text{PO}_4^{3-}]/[\text{Cl}^-]$ ratio	$i_{\text{cor}}/\mu\text{A}\cdot\text{cm}^{-2}$	E_{cor}/V	E_b/V	b_c/mV	$P_c/\%$
0.0	13.20	-0.504	-	123	-
0.1	5.97	-0.494	-	112	54.8
0.2	1.00	-0.484	0.04	116	92.4
0.4	0.61	-0.474	0.51	115	95.4
0.6	0.51	-0.463	0.64	118	96.1
0.8	0.43	-0.457	0.60	121	96.7
1.0	0.40	-0.451	0.58	125	97.0

Table 3. Effect of $[\text{PO}_4^{3-}]/[\text{Cl}^-]$ ratio on polarization parameters for HRBF500 reinforcement in Case *IV*

$[\text{PO}_4^{3-}]/[\text{Cl}^-]$ ratio	$i_{\text{cor}}/\mu\text{A}\cdot\text{cm}^{-2}$	E_{cor}/V	E_b/V	b_c/mV	$P_c/\%$
0.0	37.90	-0.550	-	75	-
0.1	7.83	-0.541	-	74	79.3
0.6	1.29	-0.522	0.24	81	96.5
1.0	0.80	-0.523	0.40	82	97.9
2.0	0.42	-0.516	0.70	86	98.9
4.0	0.40	-0.482	0.70	85	98.9

Tables 2 and 3 list the polarization parameters obtained from Fig. 4. It should be pointed out that the cathodic Tafel slope b_c and the anodic Tafel slope b_a are the kinetics parameters of metal corrosion. The greater they are, the smaller the effect of the electric field strength of the electric double layer on the electrode reaction is, and the electrode reaction is decreased. Thus, the corrosion resistance of the metal is greater. When HRBF500 reinforcement in SCP solution was passivated, the value of b_a was close to infinite, and thus it is unnecessary to discuss this fact here. The cathodic process is controlled by the activation polarization, and b_c can be used to estimate the reaction rate of HRBF500 reinforcement. The Tafel slope b_c and the effect coefficient of the electric field strength of the electric double layer on the electrode reaction α are related as follows [37, 46]:

$$b_c = 2.3\beta_c = 2.3 \times \frac{RT}{\alpha nF} \quad (6)$$

Here, R , T and F have the same meaning as in Mott–Schottky theory or the Nernst equation and n is the number of electrons transferred in the cathodic reduction reaction of oxygen:



Thus, n is four.

In Cases *III* and *IV* without phosphate, i_{cor} of HRBF500 reinforcement is very high, up to 13.2 and 37.9 $\mu\text{A}\cdot\text{cm}^{-2}$, respectively (Tables 2 and 3). The breakdown potential of the corrosion products' layer E_b does not exist. The corrosion of HRBF500 reinforcement is very severe (Figs. 2(c) and (d)). In the presence of phosphate, i_{cor} is substantially decreased, by about one or two orders of magnitude, and E_{cor} is shifted considerably in the positive direction. E_b also appears for a $[\text{PO}_4^{3-}]/[\text{Cl}^-]$ ratio of up to 0.2 in Case *III* and 0.6 in Case *IV*. With an increase in $[\text{PO}_4^{3-}]/[\text{Cl}^-]$ ratio in both cases, i_{cor} first rapidly decreases and then largely stabilized, while E_b is strongly enhanced.

There were some notable differences in the values of i_{cor} of HRBF500 reinforcement between Cases *III* and *IV* (Tables 2 and 3). In Case *III*, the changes in i_{cor} with $[\text{PO}_4^{3-}]/[\text{Cl}^-]$ ratio are reduced when the $[\text{PO}_4^{3-}]/[\text{Cl}^-]$ ratio was more than 0.4. In Case *IV*, however, the variation in i_{cor} with $[\text{PO}_4^{3-}]/[\text{Cl}^-]$ ratio is still obvious when the $[\text{PO}_4^{3-}]/[\text{Cl}^-]$ ratio was less than 1.0. In Case *III* with a $[\text{PO}_4^{3-}]/[\text{Cl}^-]$ ratio of 0.2, i_{cor} decreases to 1.00 $\mu\text{A}\cdot\text{cm}^{-2}$, while in Case *IV*, with a $[\text{PO}_4^{3-}]/[\text{Cl}^-]$ ratio of 0.6, i_{cor} is still up to 1.29 $\mu\text{A}\cdot\text{cm}^{-2}$. At $[\text{PO}_4^{3-}]/[\text{Cl}^-] = 1.0$, i_{cor} diminishes to 0.40 $\mu\text{A}\cdot\text{cm}^{-2}$ in Case *III*, while it is up to 0.80 $\mu\text{A}\cdot\text{cm}^{-2}$ in Case *IV*. When the $[\text{PO}_4^{3-}]/[\text{Cl}^-]$ ratio was increased to 4.0, i_{cor} decreases to 0.40 $\mu\text{A}\cdot\text{cm}^{-2}$ in Case *IV*. Therefore, in more aggressive environments, i.e. the combined action of carbonation and chloride-intrusion of the SCP solution in Case *IV*, a higher $[\text{PO}_4^{3-}]/[\text{Cl}^-]$ ratio is required to obtain a similar corrosion inhibition of phosphate for HRBF500 reinforcement.

E_{cor} , E_b and b_c in Cases *III* and *IV* also show some discrepancies (Tables 2 and 3). In general, E_{cor} in Case *IV* is more negative than in Case *III*. Also, the corrosion tendency of HRBF500 reinforcement in Case *IV* is larger. For the same i_{cor} , E_b in Case *IV* is greater than in Case *III*. This could be due to the fact that a higher equilibrium potential is required for the oxidation reaction of hydroxyl ions to oxygen in Case *IV*. The values of b_c in Cases *III* and *IV* are approximately 123 and 75 $\text{mV}\cdot\text{dec}^{-1}$, respectively. Therefore, α in Cases *III* and *IV* is 0.12 and 0.20, respectively. This indicates that the cathodic corrosion process of HRBF500 reinforcement in Case *III* is slightly weaker than that in Case *IV*. Moreover, the addition of phosphate inhibitor hardly changes the degree of

influence of the electric field strength on the reduction reaction of oxygen. That is, phosphate inhibitor has little influence on the cathodic corrosion process of HRBF500 reinforcement in aggressive concrete. This also implies that phosphate acts mainly as an anodic inhibitor for HRBF500 reinforcement.

With increasing in $[PO_4^{3-}]/[Cl^-]$ ratio, the efficiency of corrosion inhibition P_e of phosphate for HRBF500 reinforcement first improves considerably in both cases and then gradually stabilizes (Tables 2 and 3). The P_e value ranges up to 97.0% and 98.9% in Cases III and IV, respectively. It should be pointed out that P_e in Case III is slightly less than in Case IV, which might be due to a slightly smaller value of i_{cor} in Case III.

3.3 Effect of $[PO_4^{3-}]/[Cl^-]$ ratio - EIS measurements

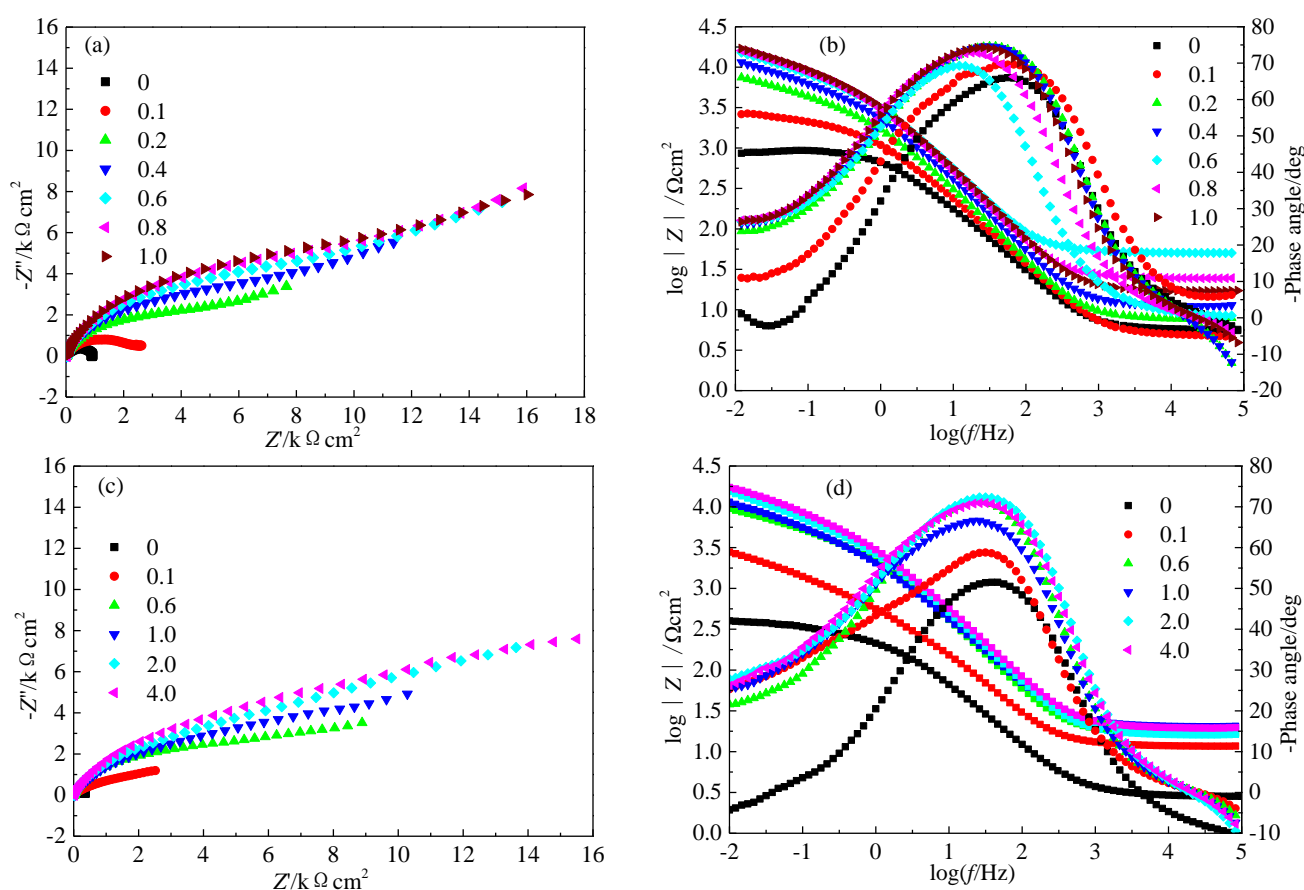


Figure 5. Effect of $[PO_4^{3-}]/[Cl^-]$ ratio on EIS diagrams for HRBF500 reinforcement: (a) Nyquist diagrams and (b) Bode diagrams in Case III; (c) Nyquist diagrams and (d) Bode diagrams in Case IV

The effect of $[PO_4^{3-}]/[Cl^-]$ ratio on EIS diagrams for HRBF500 reinforcement in Cases III and IV is shown in Fig. 5. In the absence of phosphate, the arc size in Nyquist diagrams and the impedance modulus in Bode diagrams are both very small. The electrochemical impedance value of HRBF500 reinforcement is extremely small. The peak values of the negative phase angle in Cases III and IV is

about 60° and 50° , respectively. If the corrosion products on the surface of the metal are smoother and more compact, the capacitors of the electric double layer of metal/electrolyte and the corrosion product layer will be more similar to the flat-plate capacitor and the peak of the negative phase angle will be closer to 90° [37, 47]. Thus, a low value of the peak of the negative phase angle implies a serious deformation of two kinds of capacitors on the surface of HRBF500 reinforcement. This is correlated with the cracked and loose corrosion products in Cases *III* and *IV* (Figs. 3(c) and (d)).

In the presence of phosphate in both cases, the impedance of HRBF500 reinforcement increases considerably. Thus, the charge transfer resistance of the electric double layer and the layer resistance of the corrosion products are both considerably improved. The negative peak of the phase angle is also enhanced and shifts in the low-frequency direction. The distortion of the capacitors of the electric double layer and the corrosion product layer is decreased, and the corresponding capacitance value is reduced. The capacitance value of the flat-plate capacitor is proportional to the dielectric constant and the relative plate area and inversely proportional to the plate distance. The more compact and smoother the corrosion products are, the smaller the actual area of the capacitors is. The more complete and thicker the corrosion products on HRBF500 reinforcement are, the larger the plate spacing is. Therefore, a reduction in capacitance value is intimately correlated with thicker and more compact corrosion products on the surface of HRBF500 reinforcement following addition of phosphate inhibitor (Fig. 6), which is clearly different from that without phosphate (Figs. 3(c) and (d)).

As shown in Fig. 5, the impedance in Case *III* first increases rapidly with $[\text{PO}_4^{3-}]/[\text{Cl}^-]$ ratio and then stabilizes when the $[\text{PO}_4^{3-}]/[\text{Cl}^-]$ ratio reached to 0.6, while in Case *IV* it maintains a constant increase even though the $[\text{PO}_4^{3-}]/[\text{Cl}^-]$ ratio reached to 4.0. At a $[\text{PO}_4^{3-}]/[\text{Cl}^-]$ ratio of 1.0, the impedances in Cases *III* and *IV* are approximately 17.0 and $11.3 \text{ k}\Omega\cdot\text{cm}^2$, respectively. The corresponding peak values of the negative phase angle are about 74.1 and 66.6° , respectively. The EIS indexes in the former case with phosphate are also improved. In general, these results tally with the polarization results.

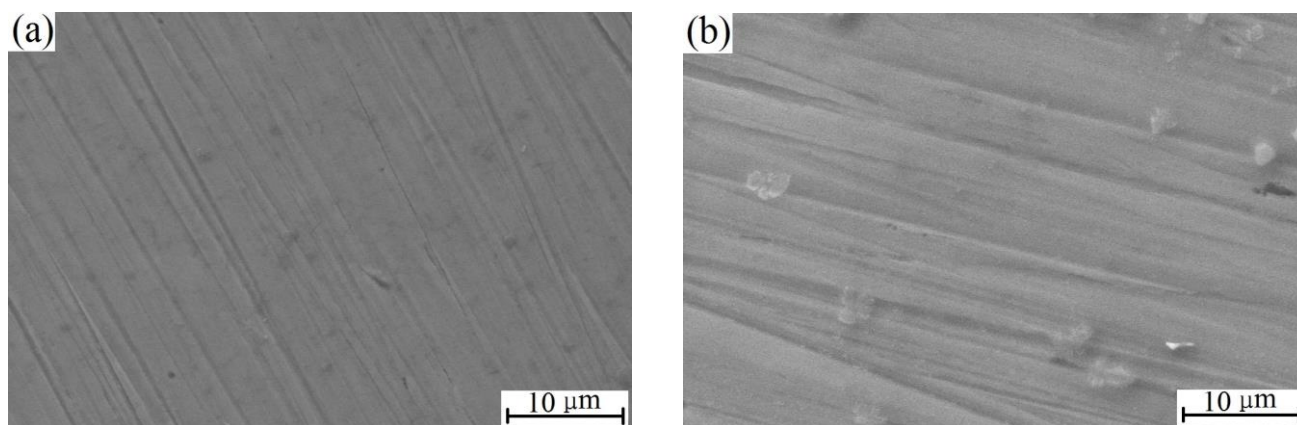


Figure 6. Effect of phosphate inhibitor on SEM images of HRBF500 reinforcement immersed in (a) Case *III* and (b) Case *IV*

3.4 Effect of $[\text{PO}_4^{3-}]/[\text{Cl}^-]$ ratio - Mott-Schottky curves

Figure 7 shows the effects of $[\text{PO}_4^{3-}]/[\text{Cl}^-]$ ratio on Mott–Schottky curves for HRBF500 reinforcement in Cases *III* and *IV*. In a large potential range the slopes of the Mott–Schottky curves are positive, indicating that the corrosion products on HRBF500 reinforcement in this potential region are n-type semiconductors. The addition of phosphate inhibitor does not vary the semiconductor type. The Mott–Schottky curves with positive slopes consist of two line segments, i.e. a low-potential range of -0.6 to -0.4 V and a high-potential range of 0 to 0.4 V. This could be due to the fact that the corrosion products have two kinds of donor concentrations [48-50]. Chen et al. [43] found that Fe and O are the major elements in passivation film on the surface of reinforcement and that Fe exists mainly in the form of Fe^{3+} and Fe^{2+} . Here, both Fe^{2+} and Fe^{3+} oxides are n-type semiconductors [50-52]. Thus, the slopes of the Mott–Schottky curves are positive. The capacitance response of the corrosion products in the low-potential range is controlled by Fe^{2+} oxides, corresponding to the shallow donor concentration N_{D1} , while that in the high-potential range is controlled by Fe^{3+} oxides, corresponding to the deep donor concentration N_{D2} . Besides Fe^{2+} and Fe^{3+} , the oxygen holes in oxides also involve in electric conduction.

According to Equation (2), the higher the slope is, the smaller the donor concentration N_D and the more compact the corrosion products are. As shown in Fig. 7, with increase in the $[\text{PO}_4^{3-}]/[\text{Cl}^-]$ ratio, the slope in Cases *III* and *IV* increases and the degree of enhancement in Case *III* is greater. Therefore, addition of phosphate inhibitor makes the corrosion products on HRBF500 reinforcement be more compact and complete.

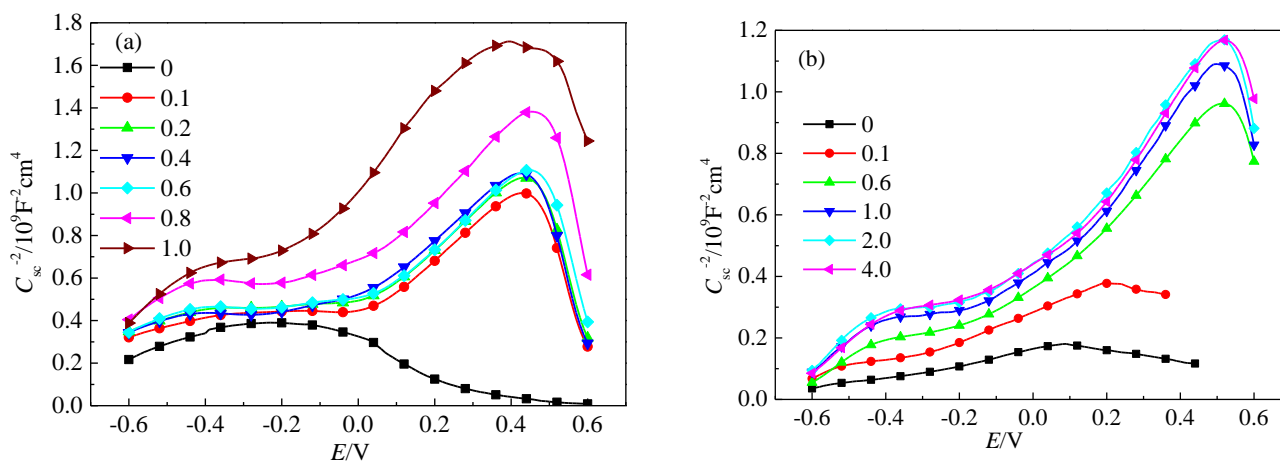


Figure 7. Effect of $[\text{PO}_4^{3-}]/[\text{Cl}^-]$ ratio on Mott–Schottky curves for HRBF500 reinforcement in (a) Cases *III* and (b) Case *IV*

There are three clearly different curves in Fig. 7. In Case *III* without phosphate (Fig. 7(a)), the high-potential range corresponded to deep donor concentration of Fe^{3+} oxides has completely disappeared. This indicates that the corrosion products possibly do not have Fe^{3+} oxides. In Case *IV* with $[\text{PO}_4^{3-}]/[\text{Cl}^-]$ ratios of 0 and 0.1 (Fig. 7(b)), two line segments related to Fe^{3+} and Fe^{2+} oxides exist, but the corresponding regions have decreased. This suggests that the corrosion products contain

both Fe^{2+} and Fe^{3+} oxides but that both the thickness and the iron content are reduced. This is in good agreement with the literature [43], which reported that the Fe^{2+} content is increased and the Fe^{3+} content is decreased in the presence of chloride and carbonation. Furthermore, the slopes in these three cases are much smaller, whereas N_D is very much greater. Therefore, the defects in corrosion products are larger (Figs. 3(c) and (d)).

Tables 4 and 5 list the N_D and E_{fb} values of the corrosion products on HRBF500 reinforcement in Cases III and IV for different $[\text{PO}_4^{3-}]/[\text{Cl}^-]$ ratios. The magnitude of N_{D1} is 10^{-20} cm^{-3} and that of N_{D2} is 10^{-19} cm^{-3} . The Fe^{2+} holes and the oxygen holes in Fe^{2+} oxides are much greater, by about one order of magnitude, than those in Fe^{3+} oxides. Therefore, the corrosion products on reinforcement with a greater content of Fe^{3+} oxides are of benefit to enhance corrosion resistance, while a greater content of Fe^{2+} oxides leads to a decrease in corrosion resistance. This is consistent with the literature [43, 52].

Table 4. Effect of $[\text{PO}_4^{3-}]/[\text{Cl}^-]$ ratio on values of N_D and E_{fb} for the corrosion products on HRBF500 reinforcement in Case III

$[\text{PO}_4^{3-}]/[\text{Cl}^-]$ ratio	Low-potential interval		High-potential interval	
	$N_{D1}/(\times 10^{20} \text{ cm}^{-3})$	E_{fb1}/V	$N_{D2}/(\times 10^{19} \text{ cm}^{-3})$	E_{fb2}/V
0.0	2.03	-0.98	–	–
0.1	2.76	-1.34	7.77	-0.23
0.2	2.23	-1.25	7.50	-0.25
0.4	2.19	-1.23	7.69	-0.29
0.6	1.77	-1.11	7.20	-0.23
0.8	1.10	-0.97	6.46	-0.31
1.0	0.79	-0.85	5.21	-0.43

For a $[\text{PO}_4^{3-}]/[\text{Cl}^-]$ ratio less than 0.4 in Case III, phosphate inhibitor hardly changes the N_{D1} value, and the N_{D2} value is also at a higher level (Table 4). With increasing $[\text{PO}_4^{3-}]/[\text{Cl}^-]$ ratio, the N_{D1} and N_{D2} values decreases significantly. This implies that in order to obtain compact corrosion products with fewer defects and smaller N_D values, the addition of phosphate is sufficient. Compared with the absence of phosphate, the reduction in the value of N_{D1} at a $[\text{PO}_4^{3-}]/[\text{Cl}^-]$ ratio of 1.0 is more than double.

Table 5. Effect of $[\text{PO}_4^{3-}]/[\text{Cl}^-]$ ratio on values of N_D and E_{fb} for the corrosion products on HRBF500 reinforcement in Case IV for different $[\text{PO}_4^{3-}]/[\text{Cl}^-]$ ratios

$[\text{PO}_4^{3-}]/[\text{Cl}^-]$ ratio	Low-potential interval		High-potential interval	
	$N_{D1}/(\times 10^{20} \text{ cm}^{-3})$	E_{fb1}/V	$N_{D2}/(\times 10^{19} \text{ cm}^{-3})$	E_{fb2}/V
0.0	5.89	-0.767	44.10	-0.592
0.1	2.48	-0.742	25.20	-0.586
0.6	1.53	-0.669	8.77	-0.202
1.0	1.25	-0.694	7.49	-0.185
2.0	1.19	-0.693	7.03	-0.180
4.0	1.19	-0.683	6.72	-0.154

With an increase in $[\text{PO}_4^{3-}]/[\text{Cl}^-]$ ratio in Case *IV*, the N_{D1} and N_{D2} values both decrease considerably (Table 5). Compared with the absence of phosphate, the N_{D1} and N_{D2} values at $[\text{PO}_4^{3-}]/[\text{Cl}^-] = 1.0$ decrease by more than four and five times, respectively. At higher $[\text{PO}_4^{3-}]/[\text{Cl}^-]$ ratios, the decrease is up to five and six times, respectively. The decrease in N_{D1} and N_{D2} values by phosphate inhibitor for HRBF500 reinforcement in Case *IV* is greater than those in Case *III*. This is similar to the P_e results (Tables 2 and 3). However, at the same $[\text{PO}_4^{3-}]/[\text{Cl}^-]$ ratio, the values of N_{D1} and N_{D2} in Case *IV* are generally greater than those in Case *III*, similar to the change in i_{cor} (Tables 2 and 3).

With an adequate addition of phosphate inhibitor, the N_D of the corrosion products on the surface of HRBF500 reinforcement decreases considerably, and the defects and impurities in corrosion products are also greatly diminished; the film is more compact and complete (Fig. 6).

Based on the point defect model (PDM) [52-54], both the growth rate and the dissolution rate of the passivation film are in a state of dynamic equilibrium. In electrolyte solutions containing chloride ions, the oxygen holes at the interface of the film/solution will absorb chloride and react with Mott-Schottky pairs to form oxygen hole/metal-ion hole pairs. The newly formed oxygen holes will continue to react with chloride ions, generating more metal-ion holes, and the reactions will continue to recycle. The redundant metal-ion holes will accumulate at the metal/film interface, leading to the cessation of film growth. Thus, the dynamic equilibrium of the growth and dissolution of the passivation film will be damaged, and the passivation film will merely be dissolved. Finally, the complete dissolution of the local passivation film will result in the occurrence and development of pitting corrosion. Therefore, more oxygen holes and metal-ion holes (i.e. higher carrier concentrations) in the passivation film will promote easier destruction of the film.

3.5 Effect of phosphate inhibitor on morphology

Figure 6 shows the effect of phosphate inhibitor on morphology of HRBF500 reinforcement immersed in Cases *III* and *IV*. In Case *III* (Fig. 6(a)) with a $[\text{PO}_4^{3-}]/[\text{Cl}^-]$ ratio of 1.0, the cracked worm spots and convex points on HRBF500 reinforcement are disappeared. The entire surface is smooth and compact, very similar to that in Case *I* which is without chloride-intrusion and carbonation (Fig. 3(a)). According to EDS analysis, a great deal of oxygen is observed, but almost no chloride is detected.

In Case *IV* (Fig. 6(b)) with a $[\text{PO}_4^{3-}]/[\text{Cl}^-]$ ratio of 4.0, the corrosion pits and flocculent corrosion products are also almost vanished, and a compact and thick layer of corrosion products is formed on the surface of HRBF500 reinforcement, considerably different from that in Case *IV* without phosphate inhibitor (Fig. 3(d)). However, there are few bulk corrosion products, which is possibly due to an inadequate rinse following corrosion immersion.

Therefore, either in a chloride-intrusion environment or in the combined chloride-intrusion and carbonation environment, a continuous and complete layer of corrosion products with smaller defects could be formed on the surface of HRBF500 reinforcement when a sufficiently high concentration of phosphate inhibitor was added to concrete.

4. CONCLUSIONS

The corrosion of HRBF500 reinforcement in SCP solutions with chloride-intrusion ($0.6 \text{ mol}\cdot\text{L}^{-1} \text{ Cl}^-$), carbonation (pH 10.5) and the combined action of chloride-intrusion ($0.3 \text{ mol}\cdot\text{L}^{-1} \text{ Cl}^-$) and carbonation (pH 10.5) was investigated for the first time. Chloride-intrusion, especially the combined action of chloride-intrusion and carbonation, leads to a serious damage of the passivation film on HRBF500 reinforcement. For the latter case, i_{cor} ranges in value up to $37.9 \mu\text{A}\cdot\text{cm}^{-2}$, N_{D} of the corrosion products is also very high, about $5.89 \times 10^{20} \text{ cm}^{-3}$, pit corrosion is very severe, and the corrosion products are both fewer and very loose.

Phosphate was then used as corrosion inhibitor for HRBF500 reinforcement in the above cases. The anodic corrosion process is substantially inhibited, while the cathodic process is only slightly so. The corrosion products still manifests as n-type semiconductors. With increase in the $[\text{PO}_4^{3-}]/[\text{Cl}^-]$ ratio, i_{cor} rapidly decreases and then stabilizes, N_{D} and the defects in corrosion products are markedly reduced. With sufficient phosphate inhibitor, the corrosion products on HRBF500 reinforcement are compact and complete, similar to those without any contaminants.

The efficiency of inhibition by phosphate for HRBF500 reinforcement in chloride-intrusion and combined chloride-intrusion and carbonation has some notable differences. At the same $[\text{PO}_4^{3-}]/[\text{Cl}^-]$ ratio, the electrochemical indexes in the former case are generally superior to those in the latter case. For example, in the former case, i_{cor} decreases to $0.40 \mu\text{A}\cdot\text{cm}^{-2}$ at a $[\text{PO}_4^{3-}]/[\text{Cl}^-]$ ratio of 1.0, while i_{cor} is up to $0.80 \mu\text{A}\cdot\text{cm}^{-2}$ for the latter case and declines to $0.42 \mu\text{A}\cdot\text{cm}^{-2}$ at $[\text{PO}_4^{3-}]/[\text{Cl}^-] = 4.0$. Therefore, a greater concentration of phosphate inhibitor for HRBF500 reinforcement is demanded under the combined action of carbonation and chloride-intrusion of the SCP solution.

The effect of phosphate inhibitor for HRBF500 reinforcement in actual concrete will also be investigated in future studies.

ACKNOWLEDGEMENTS

This work was financially supported by the National Nature Science Foundation of China (Nos. 51408517 and 51578255) and the Nature Science Foundation of Fujian Province.

References

1. R. Lahdo, O. Seffer, A. Springer, S. Kaielerle and L. Overmeyer, *Physics Procedia*, 56 (2014) 637.
2. W. Chen, Z. Shi, Y. Zhao and Y. M. Yu, *T. Mater. Heat Treat.*, 31 (2010) 77.
3. X. L. Li, Z. H. Guo, Y. H. Rong, H. Y. Wu and S. F. Yao, *Acta Metall. Sin.*, 50 (2014) 439
4. W. B. Lv, *Microstructure and properties of fine grains for high strength hot rolled bars*, Northeastern Univ., 2010, Shenyang, China
5. X. L. Wang, H. Z. Gao and K. Li, *J. Zhengzhou Univ. (Eng. Sci.)*, 33 (2012) 1.
6. 'Code for design of concrete structures [S]', GB50010-2010, Beijing, China, 2010.
7. Q. F. Wang, H. C. Wu, Y. Y. Xu and Z. Y. He, *J. Build. Struc.*, 32 (2011) 120.
8. J. J. Zhao, Q. X. Zhang, Y. X. Yang, M. Yang and J. Lian, *J. B. Univ. Technol.*, 39 (2009) 52.
9. B. N. Li, H. Dai and J. W. Zhang, *J. Southeast U.: Nat. Sci. Ed.*, 44 (2014) 832.
10. B. L. Lin and Y. Y. Xu, *Int. J. Electrochem. Sci.*, 11 (2016) 3824.
11. T. Ruan, N. Spandley, C. Johnson and A. Poursae, *Fire Safety J.*, 78 (2015) 196.
12. N. Etteyeb and X. R. Nóvoa, *Corros. Sci.*, 112 (2016) 471.

13. G. Z. Meng, Y. Li, Y. W. Shao, T. Zhang, Y. Q. Wang, F. H. Wang, X. Q. Cheng, C. F. Dong and X. G. Li, *J. Mater. Sci. Technol.*, 32 (2016) 465.
14. A. Abbasi Aghuy, M. Zakeri, M. H. Moayed and M. Mazinani, *Corros. Sci.*, 94 (2015) 368.
15. J. L. S. Ribeiro, Z. Panossian and S. M. S. Selmo, *Constr. Build. Mater.*, 40 (2013) 40.
16. L. Yohai, M. Vázquez and M. B. Valcarce, *Electrochim. Acta*, 102 (2013) 88.
17. Y. S. Wang, Y. Zuo, X. H. Zhao and S. S. Zha, *Appl. Surf. Sci.*, 379 (2016) 98.
18. M. M. Mennucci, E. P. Banczek, P. R. P. Rodrigues and I. Costa, *Cem. Concr. Compos.*, 31 (2009) 418.
19. B. Qiao, R. G. Du, W. Chen, Y. F. Zhu and C. J. Lin, *Acta Metall. Sin.*, 46 (2010) 245.
20. J. J. Shi, W. Sun and G. Q. Geng, *Acta Metall. Sin.*, 47 (2011) 449.
21. T. U. Mohammed, N. Otsuki and M. Hisada, *J. Mater. Civil Eng.*, 13 (2001) 194.
22. J. H. Jiang, Y. S. Yuan, F. M. Li, B. Wang and Y. S. Ji, *J. Build. Mater.*, 12 (2009) 523.
23. W. Z. Gan, W. L. Jin and T. Y. Xu, *J. Build. Mater.*, 12 (2009) 699.
24. G. Li, X. M. Dalang and Y. S. Yuan, *J. China Min. Techno.*, 38 (2009) 149.
25. J. J. Shi, W. Sun, G. Q. Geng and P. Jiang, *J. Univ. Sci. Technol. B.*, 33 (2011) 1471.
26. B. L. Lin and Y. Y. Xu, *J. Build. Mater.*, 19 (2016) 1082.
27. B. L. Lin and Y. Y. Xu, International Conference on Electronic & Mechanical Engineering and Information Technology, Haerbin, 2011, 5: 2328.
28. Y. Y. Xu and B. L. Lin, *Appl. Mech. Mater.*, 105–107 (2012) 1797.
29. S. M. Abd El Haleem, S. Abd El Wanees and A. Bahgat, *Corros. Sci.*, 87 (2014) 321.
30. F. T. Cao, J. Wei, J. H. Dong and W. Ke, *Corros. Sci.*, 100 (2015) 365.
31. F. L. Fei, J. Hu, J. X. Wei, Q. J. Yu and Z. S. Chen, *Constr. Build. Mater.*, 70 (2014) 43.
32. B. Elsener and U. Angst, *Corrosion inhibitors for reinforced concrete: Science and Technology of Concrete Admixtures*, Elsevier, 2016, Amsterdam, Holland.
33. C. Xu, W. L. Jin, H. L. Wang, H. T. Wu, N. Huang, Z. Y. Li and J. H. Mao, *Constr. Build. Mater.*, 115 (2016) 602.
34. L. Yohai, W. Schreiner, M. Vázquez and M. B. Valcarce, *Electrochim. Acta*, 202 (2016) 231.
35. K. Aramaki, *Corros. Sci.*, 46 (2004) 1565.
36. I. A. Kartsonakis, S. G. Stanciu, A. A. Matei, R. H., A. Karantonis and C. A. Charitidis, *Corros. Sci.*, 112 (2016) 289.
37. C. N. Cao, *Principles of electrochemistry of corrosion*, Chemical Industry Press, 2008, Beijing, China.
38. M. J. Pryor and M. Cohen, *J. Electrochem. Soc.*, 100 (1953) 203.
39. T. A. Söylev and M. G. Richardson, *Constr. Build. Mater.*, 22 (2008) 609.
40. A. La Iglesia, V. M. La Iglesia, S. Fajardo, P. P. Gómez and J. M. Bastidas, *Constr. Build. Mater.*, 37 (2012) 46.
41. D. M. Bastidas, M. Criado, V. M. La Iglesia, S. Fajardo, A. La Iglesia and J. M. Bastidas, *Cem. Concr. Compos.*, 43 (2013) 31.
42. H. Nahali, L. Dhouibi and H. Idrissi, *Constr. Build. Mater.*, 50 (2014) 87.
43. W. Chen, R. G. Hu, H. Y. Shi, Y. F. Zhu and C. J. Lin, *Acta Metall. Sin.*, 47 (2011) 735.
44. E. Zitrou, J. Nikolaou, P. E. Tsakiridis and G. D. Papadimitriou, *Constr. Build. Mater.*, 21 (2007) 1161.
45. S. R. Morrison and H. H. Wu, *Electrochemistry at semiconductor and oxidized metal electrodes*, Science Press, 1988, Beijing, China.
46. J. O. Bird and P. J. Chivers, *Electrode potentials, cells and corrosion: Newnes Engineering and Physical Science Pocket Book*, Elsevier, 1993, Amsterdam, The Netherlands.
47. A. V. Benedetti, P. T. A. Sumodjo, K. Nobe, P. L. Cabot and W. G. Proud, *Electrochim. Acta*, 40 (1995) 2657.
48. Q. Wu, Y. Liu, R. G. Du and C. J. Lin: *Acta Metall. Sin.*, 44 (2008) 346.
49. M. Sukhotin, M. S. Grilikhes and E. V. Lisovaya, *Electrochim. Acta*, 34 (1989) 109.

50. J. Luo, Y. Wang, J. B. Jiang, Q. D. Zhong, Z. Y. Zhu and L. Zhang, *Acta Chim. Sin.*, 70 (2012) 1213.
51. W. Jon and O. B. Isgor, *Corros. Sci.*, 106 (2016) 82.
52. D. G. Li, D. R. Chen, Y. R. Feng, Z. Q. Bai and M. S. Zheng, *Acta Chim. Sin.*, 66 (2008) 2329.
53. D. D. Macdonald, *J. Electrochem. Soc.*, 139 (1992) 3434.
54. X. Zhou, R. Chen, H. Y. Yang and F. H. Wang, *J. Chin. Soc. Corros. Prot.*, 34 (2014) 125.

© 2017 The Authors. Published by ESG (www.electrochemsci.org). This article is an open access article distributed under the terms and conditions of the Creative Commons Attribution license (<http://creativecommons.org/licenses/by/4.0/>).